

Soft particle model for block copolymers

F. Eurich¹, A. Karatchentsev¹, J. Baschnagel², W. Dieterich¹, P. Maass³

¹*Fachbereich Physik, Universität Konstanz, D-78457 Konstanz, Germany*

²*Institut Charles Sadron, 6 rue Boussingault, Strasbourg, Cedex 67083, France and*

³*Fakultät für Mathematik und Naturwissenschaften,*

Technische Universität Ilmenau, Postfach 100565, 98648 Ilmenau, Germany

A soft particle model for diblock (AB) copolymer melts is proposed. Each molecule is mapped onto two soft spheres built by Gaussian *A*- and *B*-monomer distributions. An approximate analytical expression for the joint distribution function for the distance between both spheres and their radii of gyration is derived which determines the entropic contribution to the intramolecular free energy. Adding a mean-field expression for the intermolecular interactions, we obtain the total free energy of the system. Based on this free energy, Monte Carlo simulations are carried out to study the kinetics of microphase ordering in the bulk and its effect on molecular diffusion. This is followed by an analysis of thin films with emphasis on pattern transfer from walls with a periodic structure. It is shown that the level of coarse graining in the soft particle model is suitable to describe structural and kinetic properties of copolymers on mesoscopic scales.

1. Introduction

Coarse graining by elimination of irrelevant degrees of freedom is a central problem in many areas of statistical physics, especially when modelling diffusion and the phase kinetics in polymer systems.¹ An important class of processes is phase separation in polymer melts with incompatible components, which occur on time and length scales many orders of magnitude larger than those related to the motion of individual monomers. A detailed understanding of such processes is required in present-day attempts to utilize polymers in the design of new materials and in the production of tailored micro- or nanoscale structures by self-organization.^{1,2}

From the theoretical viewpoint this poses the problem to eliminate internal degrees of freedom of polymer chains, and to seek for a coarse grained description of the kinetics in terms of a small number of collective degrees of freedom. In order to cover effects of chain length, monomer interactions, heterogeneities in monomer sequences e.g. in the case of copolymers, and interactions with walls in confined systems,³ such coarse grained theories should be based on appropriate microscopic input.

A promising approach is to represent polymer chains in their coil conformation in dense systems simply by interpenetrating “soft particles”. This soft-particle picture should be applicable for length scales comparable to or larger than the radius of gyration R_G and for time scales of the order of the diffusion time $\tau_D \simeq R_G^2/D$, where D denotes the center of mass diffusion constant. The soft geometrical object assigned to a polymer can be quite general and should be characterized by only a few parameters. In the simplest case, polymers are described by soft spheres with effective interactions that can be derived by an explicit elimination procedure for monomer degrees of freedom.⁴ Slightly more complex geometrical objects are soft ellipsoids, which allow one to take into account orientational effects and anisotropic shape deformations. For homopolymers the first soft-ellipsoid model was developed in Ref.⁵ based on microscopic input de-

rived from a bead spring model. This model includes the excluded volume effect into the effective intramolecular free energy. As a consequence, tuning of interaction parameters with control parameters (temperature, degree of polymerization) is necessary to capture correctly the screening effect responsible for the quasi-ideal chain behavior in dense systems. It was shown that this adaption of effective interaction parameters can be avoided by using the Gaussian chain model as basis for the soft ellipsoid model,⁶ at the expense that the excluded volume effect in this model has to be included in a mean field type manner in the self-interacting term of the free energy. Based on the Gaussian ellipsoid model, structural and kinetic properties of both one-component melts and binary mixtures were studied successfully for bulk systems. In a subsequent extension to confined systems it was shown how spinodal decomposition in polymer blends becomes modified in thin films, including situations of periodically patterned walls.⁷

Soft particle models become increasingly valuable in the description of complex matter systems, and also analytical techniques can be used to relate the input parameters to microscopic properties.^{8,9}

In this paper we propose a soft particle model for block copolymers. Phase separation in these systems proceeds under the constriction of a chemical link between incompatible polymer blocks.^{10,11} Depending on the relative amounts of different blocks, a variety of ordered microphases can emerge on length scales that are tunable by the respective degrees of polymerization. Because of these unique features block copolymers offer a promising tool for the fabrication of nanoscale devices as, for example, by the nanolithography technique.^{12,13}

Following the early fundamental work on the derivation of a Landau theory by Leibler¹⁴ and of fluctuation corrections by Ohta and Kawasaki¹⁵ and subsequently by Fredrickson and Helfand,¹⁶ a progressive understanding of the phase diagram of diblock-copolymers with variable length ratio of the two blocks has been developed. Important features like the static structure fac-

tor and the scaling of the microphase periodicity with chain length were examined by the lattice Monte Carlo technique.^{17,18,19} Further simulation studies provided insight into the detailed changes of chain conformation near phase boundaries,^{20,21,22} the internal energy and entropy,²³ as well as transport properties, e.g. center-of-mass diffusion of chains and their modification by the order-disorder transition.^{19,22} More sophisticated methods are the “dissipative particle dynamics” (DPD) that includes hydrodynamic forces between effective beads of polymers,^{24,25} and methods treating the entangled state of copolymers.²⁶

On the other hand, for studying the far-from-equilibrium dynamics and large scale structures, evolution equations for monomer densities have been developed. One approach is to formulate time-dependent Ginzburg-Landau (TDGL) equations.^{27,28,29,30} A powerful extension thereof is the selfconsistent (SFC) field method,^{31,32} which proved successful in predicting large scale phase morphologies.

Complementary to these developments is the soft particle model proposed here. Motivated by the results of Refs.^{6,7} we explore the possibility to map the internal molecular degrees of freedom onto only a few parameters, allowing straightforward physical interpretation. In other words, we attempt to coarse-grain as far as possible while keeping the most important structural characteristics of individual molecules. Because of its simplicity, this model should enable one to treat the time evolution of ordering structures, including surface-induced structures, in an efficient manner. Unlike TDGL or SCF theories, it retains orientational effects and shape fluctuations of individual molecules, features which again will be important when treating surface effects. Moreover, a model of this type could form the basis for treating the phase behavior of more complex molecules.

Our paper is organized as follows. First, we develop in section 2 a soft-particle model of (AB)-diblock copolymers, where each block is represented by a Gaussian sphere. Their radii of gyration R_X ($X = A, B$) and the vector \vec{r} connecting their midpoints are the only parameters related to the internal degrees of freedom of a molecule. Test calculations for the structure factor, the ordering transition, the scaling of the lamellar distance, stretching of chains, as well as diffusion properties in the bulk are presented in section 3. Thereby we demonstrate that this Gaussian disphere model (GDM) reproduces known bulk properties in a satisfactory manner. This motivates us to treat in section 4 equilibrium and kinetic properties in thin film geometries. Major questions concern the wall-induced microphase separation both for neutral walls and walls that attract one component, and the dynamics of pattern transfer from prepatterned walls into the film. Finally, some concluding remarks and directions for further research are presented in section 5.

2. Gaussian disphere model for block copolymers

Following the basic idea in previous work³³ we propose here to represent each block in an (AB)-diblock copolymer molecule by one soft sphere with radius of gyration R^X ($X = A$ or B), as illustrated in Fig. 1. The molecules’ orientation is given by the vector $\vec{r} = \vec{r}^A - \vec{r}^B$ connecting the two centers of the spheres. Its magnitude $r = |\vec{r}|$ determines the stretching of the molecule under AB-repulsion. The three quantities R^A , R^B and \vec{r} are the parameters that represent the internal degrees of freedom of one molecule. In order to express configurational fluctuations of a molecule in terms of these parameters, we have to specify

- i) the joint probability densities $P(\vec{r}, R^A, R^B)$ for given number of bonds in the A and B block, N_A and N_B , respectively.
- ii) the conditional monomer densities $\rho_X(\vec{x}|\vec{r}, R^A, R^B)$ of the block X written in terms of the coordinate \vec{x} relative to the center \vec{r}^X of the sphere. The normalization condition is

$$\int \rho_X(\vec{x}|\vec{r}, R^A, R^B) d^3x = N_X + 1. \quad (1)$$

These densities are to be derived from a microscopic model of an isolated chain. For the free energy of an ensemble of M molecules with fixed values N_A and N_B we write

$$F = F_{\text{intra}} + F_{\text{inter}}, \quad (2)$$

where

$$F_{\text{intra}} = -k_B T \sum_{i=1}^M \ln P(\vec{r}_i, R_i^A, R_i^B) \quad (3)$$

is the intramolecular part in the absence of intermolecular interactions. For the latter, contact interactions of strength ϵ_{XY} among the different blocks ($X, Y = A$ or B) are considered here,

$$F_{\text{inter}} = \frac{1}{2} \sum_{i,j=1}^M \sum_{X=A,B} \sum_{Y=A,B} \epsilon_{XY} b^3 \int d^3y \tilde{\rho}_i^X(\vec{y}) \tilde{\rho}_j^Y(\vec{y}), \quad (4)$$

where b^3 is a contact volume. The parameter b sets the microscopic length scale of the model and is used as length unit, $b = 1$. The density $\tilde{\rho}_i^X$ denotes the X -monomer density in the laboratory frame,

$$\tilde{\rho}_i^X(\vec{y}) = \rho_X(\vec{y} - \vec{r}_i^X | \vec{r}_i, R_i^A, R_i^B). \quad (5)$$

Note that we have included the self-interaction terms $i = j$ in eq. (4), which implies that we should consider entropic contributions only in F_{intra} .

To complete the definition of the free energy, we must specify the input functions P and ρ_X . Following Ref.⁶,

we propose to use Gaussian chains as microscopic input, with a few additional approximations that lead to simple analytic expressions. First we consider P . Here our assumption is that R^A and R^B are uncorrelated, with distributions $P_X(R^X)$ obtained from homogeneous Gaussian chains. Thus we can write

$$P(\vec{r}, R^A, R^B) = P_A(R^A) P_B(R^B) W(\vec{r}|R^A, R^B) \quad (6)$$

with

$$P_X(R^X) \sim \frac{1}{\sqrt{N_X}} p\left(\frac{R^X}{\sqrt{N_X}}\right), \int_0^\infty du p(u) = 1 \quad (7)$$

for large N_X . An accurate representation of the scaling function is⁶

$$p(u) = \frac{1}{uK_0(2d)} \exp\left(-\frac{u^2}{a} - d^2 \frac{a}{u^2}\right), \quad (8)$$

where $K_0(z)$ denotes the modified Bessel function of order zero and the coefficients a and d are known from fits to the exact moments of second and fourth order in the limit of large N_X ($\langle(R^X)^2\rangle \simeq N_X/6$; $\langle(R^X)^4\rangle \simeq (19/540)N_X^2$). For the conditional probability in (6), we make a Gaussian ansatz with respect to \vec{r} ,

$$W(\vec{r}|R^A, R^B) = \left(\frac{3}{2\pi\langle\vec{r}^2\rangle_R}\right)^{3/2} \exp\left(-\frac{3\vec{r}^2}{2\langle\vec{r}^2\rangle_R}\right) \quad (9)$$

where $\langle\vec{r}^2\rangle_R = 2[(R^A)^2 + (R^B)^2]$ is the variance of \vec{r} for given R^A and R^B .

As a test of (9) we compare with Monte Carlo simulations the conditional probability $W(r|R^A)$ obtained from (9) by integrating over the orientations of \vec{r} with $r = |\vec{r}|$ fixed, and by averaging over R^B . Regarding its dependence on R^A , we took averages over each of eight successive intervals on the R^A axis chosen such that they have equal weights $1/8$ with respect to the distribution (7). Results are shown in Fig. 2 by the continuous curves, together with the simulation data. With increasing R^A , peak positions move to the right, showing that chain realizations with large R^A imply larger stretchings r . The semilogarithmic plot in the inset confirms satisfactory agreement between the data and the Gaussian approximation.

Second, we turn to the conditional monomer density ρ_X . As mentioned already, we assume a spherical shape and ignore any dependence on \vec{r} and on the size of the opposite block, i.e. $\rho_X = \rho_X(\vec{x}|R^X)$. Then for large N_X and for typical R^X (excluding highly stretched chains) one can show that the scaling form

$$\rho_X(\vec{x}|R^X) \sim \frac{N_X + 1}{(R^X)^3} f\left(\frac{x}{R^X}\right) \quad (10)$$

with $f(v) = (3/2\pi)^{3/2} \exp(-3v^2/2)$ well agrees with Monte Carlo simulations for isolated chains. Using (10) as approximation in the GDM directly follows the analogous reasoning in the soft ellipsoid model, described in

detail in Ref.⁶. To complete the description of the GDM, we give the expression for the radius of gyration R_G of the total chain, to be derived by simple geometric considerations

$$R_G^2 = f_A[R^A]^2 + f_B[R^B]^2 + f_A f_B \bar{r}^2, \quad (11)$$

where $f_X = N_X/N$, and $N = N_A + N_B$. It is clear that this type of model can be extended to more complicated structures like triblock copolymers, but we will not pursue this here.

So far, for given external parameters N_X , M and V , we have constructed a free energy F that depends on the variables R_i^X and \vec{r}_i^X (giving $\vec{r}_i = \vec{r}_i^A - \vec{r}_i^B$). To model the kinetics, these variables are changed in a Monte Carlo process. Two types of elementary moves are considered: (i) block translations $\vec{r}_i^X \rightarrow \vec{r}_i^X + \Delta\vec{r}_i^X$ where the components of $\Delta\vec{r}_i^X$ are drawn from a uniform distribution in the interval $[-\Delta r_{\max}^X/2, \Delta r_{\max}^X/2]$ with $\Delta r_{\max}^X = (3/4)(N_X/6)^{1/2}$, and (ii) size changes $R_i^X \rightarrow R_i^X + \Delta R_i^X$, where ΔR_i^X is uniformly distributed in the interval $[-\Delta R_{\max}^X/2, \Delta R_{\max}^X/2]$ with $\Delta R_{\max}^X = 0.5(N_X/6)^{1/2}$ under the additional constraint $R_i^X > 0$. All elementary steps have the same a priori probability. Acceptance probabilities are chosen according to the Metropolis algorithm based on the free energy (2).

Results are presented in terms of the Flory-Huggins type parameter $\chi = (2\epsilon_{AB} - \epsilon_{AA} - \epsilon_{BB})/k_B T$ and we will use $k_B T$ as energy unit in the following, $k_B T = 1$. All calculations are performed for $\epsilon_{AA} = \epsilon_{BB} = 1$ and a total mean density of monomers $\bar{\rho} = 0.85$. Unless otherwise said, symmetric mixtures with a fraction $f_A = 0.5$ of A monomers are considered and a chain length $N = 120$ is chosen.

3. Bulk properties

In this section we test the GDM against bulk properties of chain-like copolymers, a subject well known from extensive model studies.^{14,15,16,17,18,19,20,21,22,23,24,25} We show that despite its simplicity the GDM accounts for a remarkable set of both structural and diffusion properties connected with microphase separation. In all bulk simulations periodic boundary conditions are used and the volume V of the cubic simulation box is chosen to contain in total $M = 4000$ molecules. Averages are typically performed over 10 independent simulation runs.

3.1 Structure

A direct measure of short- and long-range ordering is the static structure factor $S(\vec{k})$, which we define through the density correlation function of A-monomers,

$$S(\vec{k}) = \frac{V}{MN_A} \int d^3x \langle \rho_A(\vec{x}) \rho_A(0) \rangle e^{i\vec{k}\cdot\vec{x}}. \quad (12)$$

In Fig. 3, data points of the spherical average of (12) are displayed for symmetric chains in the disordered phase. Continuous curves are fits to the expression^{14,17}

$$NS^{-1}(k) = \frac{1}{\alpha}[F(k\tilde{R}_G) - \delta] \quad (13)$$

with

$$F(x) = \frac{x^4}{2} \left(\frac{x^2}{4} + e^{-x^2/2} - \frac{e^{-x^2}}{4} - \frac{3}{4} \right). \quad (14)$$

Equation (13) generalizes the form of the structure factor from Leibler's random phase approximation, which in our notation amounts to setting $\alpha = 1/2$, $\tilde{R}_G = R_G$ and $\delta = 2\chi N$. In this theory, lamellar ordering sets in at the critical value $(\chi N)_c^L = 10.5$, connected with a divergence of $S(k)$ at $k = k_*$ with $k_*R_G = 1.95$. Following previous work^{17,18,22} α , \tilde{R}_G and δ are regarded as fit parameters, which we determine from the behavior of $S(k)$ around its main peak at k_* . Their values are given in Table 1. In the vicinity of the peak and towards small k a good fit is achieved, whereas at larger k the data points fall below the continuous curve, see Fig. 3. This is to be expected because the intramolecular connectivity is not taken into account by assuming Gaussian monomer densities within each block.

The physical meaning of the parameters α , \tilde{R}_G , and δ is to allow for a shift in the peak position k_* relative to the Leibler value¹⁴ and a deviation of the maximum value $S(k_*)/N$ from scaling with χN . Indeed, our results in Fig. 3 reflect a downward shift in k_* with increasing χ , starting with $k_*R_G \simeq 1.8$ for $\chi = 0$. Qualitatively, this downward shift agrees with previous calculations,^{18,22} but the effect is smaller than in these works. Moreover, when plotting $NS^{-1}(k_*)$ from calculations with different N against χN , see Fig. 4, linear extrapolation to zero yields an instability of the disordered phase at a critical value $(\chi N)_c$ that increases with decreasing chain length N . This trend is qualitatively consistent with the Fredrickson and Helfand theory,¹⁶ predicting $(\chi N)_c^{\text{FH}} - (\chi N)_c^L \propto N^{-1/3}$. In our model the critical value for the longest chains ($N = 300$) is roughly estimated as $(\chi N)_c \simeq 12$ to 14.

Ordered structures spontaneously forming under a quench from the disordered state to a value χN above but still close to $(\chi N)_c$, display a multidomain pattern and weak segregation, i.e. a smooth variation of the respective monomer densities when passing from A-rich to B-rich domains. Figure 5a exemplifies the structure factor for $\chi N = 30$. The position of the sharp peak at $k_* = 2\pi/\lambda$ reflects the lamellar periodicity λ . Obviously, k_* is smaller than in the disordered state of molecules with the same chain length, due to their stretching under alignment. In the GDM, chain stretching is described by the parameter $r = \langle \vec{r}^2 \rangle^{1/2}$. Its dependence on χN (with N fixed) is plotted in Fig. 6, showing a pronounced increase in the vicinity of the ordering transition and a subsequent weaker increase as χN rises further. For $\chi = 0$,

one recovers $r^2 = 2[\langle (R^A)^2 \rangle + \langle (R^B)^2 \rangle]$, see section 2. The averaged radii of gyration $\langle (R^X)^2 \rangle^{1/2}$ of individual blocks are practically unaffected by changing χ .

Going to strong segregation, larger scale oriented lamellae with sharp interfaces develop. This leads to higher-order peaks in $S(k)$ seen in Fig. 5b, where we plotted the structure factor for $\chi N = 54$. Note the absence of the second order peak due to the arrangement of blocks inside the domains. We also carried out bulk simulations for asymmetric chains. The existence of a cylindrical phase is exemplified by Fig. 5c for $f_A = 0.3$, reflected by superstructure peaks as marked in the figure.

Computations with different combinations of χ and N in the strong segregation range allow us to test the scaling prediction for the lamellar distance $\lambda = 2\pi/k_*$ of the form $\lambda/N^{1/2} \sim (\chi N)^n$. This relation is obtained by minimizing the sum of the elastic energy due to molecular stretching and the interfacial energy within the period λ , yielding $n = 1/6$.¹ Indeed, a good collapse of data for different N and χ is achieved in the double logarithmic plot of $\lambda/N^{1/2}$ versus χN , as shown in Fig. 7. The exponent deduced from the slope of the straight line is $n \simeq 0.22$, in fair agreement with the mean field argument indicated before. For small (χN) -values corresponding to the disordered phase, a saturation is seen, i.e. $\lambda \propto N^{1/2}$.

3.2 Diffusion

As shown previously,^{18,22} the center of mass diffusion of molecules in the disordered phase slows down upon increasing χN , because of the increasing degree of short range order, reflected by the increase of $S(k_*)$. In the lamellar phase, diffusion parallel to the interfaces is quite similar as in the disordered phase near the ordering transition, whereas perpendicular diffusion gets strongly suppressed and drops to zero when χN is increased further. As seen in Fig. 8 the GDM reproduces these general features. To distinguish D_{\parallel} from D_{\perp} in the ordered phase, oriented lamellae were prepared through appropriate initial conditions. The slight increase of D_{\parallel} right above the transition point may originate from the reduction of structural fluctuations and smoothening of the interfaces. The overall diffusion coefficient is consistent with the average $D \approx (2D_{\parallel} + D_{\perp})/3 \approx (2/3)D_{\parallel}$. Analysis of the time dependent center of mass mean squared displacements showed that the directionally averaged short-time diffusion coefficients are almost unaffected by the interaction χ and are close to $D(\chi = 0)$.

An intuitive approach to understand the diffusion across the domain boundaries in the lamellar phase is to adopt the picture of one-dimensional Brownian motion in a periodic potential $V(z)$. We start from the exact expression³⁴ $D = D_0 / \left[\overline{e^{-V(z)}} \overline{e^{V(z)}} \right]$, where D_0 is the diffusion coefficient in the corresponding homogeneous state, and the bars denote averages over one period. Obviously, the rate determining diffusion steps are those

near the maximum of $V(z)$ or the minimum of the equilibrium density $\rho_{eq}(z) \propto \exp(-V(z))$. Within mean field theories³⁵ this aspect can be generalized to interacting systems by regarding $V(z)$ as potential of mean force, defined in terms of the actual equilibrium density via the Boltzmann factor. Guided by these ideas, we write for our system

$$D_{\perp} \simeq \frac{D_0}{\left[\overline{\rho_A(z) \rho_A^{-1}(z)} \right]} \quad (15)$$

with simulated A -monomer densities $\rho_A(z)$ and diffusion constant D_0 at the ordering transition point. Close to the ordering transition $\rho_A(z)$ can be represented as $\rho_A(z) \simeq \overline{\rho_A}(1 + \Delta\rho_A \sin k_* z)$, which yields $D_{\perp} = D_0(1 - \Delta\rho_A^2)^{1/2}$. This simple approach already describes the sharp drop in D_{\perp} for $\chi N > (\chi N)_c$, shown in Fig. 8. It still overestimates the simulated data for D_{\perp} especially at larger χN . One reason may lie in the fact that shape deformations of molecules during barrier crossing are not included in these arguments. The barrier crossing problem for a block copolymer has been studied in Ref.³⁶.

4. Thin films

Confinement of block copolymers between planar walls adds several new aspects to microphase separation.^{37,38,39} A common repulsion of A and B blocks by neutral walls will favor parallel orientation of molecules and therefore can induce perpendicular lamellar ordering. However, if walls act differently on A and B -monomers, one type of blocks will be preferred to the walls, favoring parallel lamellar ordering. These competing behaviors, including their time dependence under initial conditions corresponding to a disordered state at high temperatures, have been studied before. Hence we limit ourselves to a few representative and supplementary results.

Patterned walls are particularly interesting for applications, where a chemically pre-patterned surface should be translated into a correspondingly patterned polymer film.^{40,41,42} We show that the GDM can provide new insight into the process of pattern translation. Calculations of the time-dependent structure factor enable us to discuss the propagation of stripe patterns into the film and their competition with spontaneous ordering fluctuations away from the pre-patterned substrate.

In the film simulations periodic boundary conditions are used in the lateral directions. Unless otherwise specified, films have a lateral size $L_x = L_y = 4\lambda$ with λ the lamellar distance in the bulk (for example, $\lambda = 31$ for $N = 120$ and $\chi = 0.45$, see section 3). Averages are performed over typically 10 independent runs.

4.1 Homogeneous walls

We start with planar walls parallel to the (x, y) -plane, with a potential for A and B monomers as in Ref.⁷,

$$\begin{aligned} V_X^{(1)} &= \epsilon_X^{(1)} \exp\left(-\frac{z}{2l_w}\right), \\ V_X^{(2)} &= \epsilon_X^{(2)} \exp\left(-\frac{L_z - z}{2l_w}\right), \end{aligned} \quad (16)$$

where the superscript (1) refers to the lower wall at $z = 0$ and the superscript (2) to the upper wall at $z = L_z$. The quantity l_w is a parameter that tunes the softness of the confinement.²² For simplicity we have chosen it to be the same for A and B monomers and the same for both walls, $l_w = 0.5$. The exponential form of the wall-monomer interaction is convenient, since it allows one to get analytical expressions for the integrals that determine the interaction with Gaussian monomer densities.⁷

As discussed above, for neutral walls, molecules near the wall acquire a preferential parallel orientation. To show this, we set $\epsilon_A^{(j)} = \epsilon_B^{(j)} = \epsilon_w = 1$, $j = 1, 2$, and calculated the quantity $\langle |\cos \Theta(z)| \rangle$ in the equilibrium state (after thermalization), where Θ denotes the angle between the vector \vec{r} of a molecule and the z -axis. The results are shown in Fig. 9 after averages were taken over x and y for fixed z coordinate. Obviously, angles Θ near $\pi/2$ prevail near $z = 0$ and $z = L_z$. A preferred parallel orientation persists even up to the middle of the slab (random orientations would give $\langle |\cos \Theta(z)| \rangle = 0.5$). The repulsive interactions between monomers and the walls lead to a deformation of molecules close to the walls, as seen by the behavior of the average block radius of gyration versus z . At this point the neglect of the internal molecular structure in the GDM becomes apparent. Close to a wall, chain polymers have been shown to get compressed in the z -direction, but elongated in the (x, y) -plane.³⁸ Such anisotropic deformations are beyond the scope of the GDM. This sets a lower limit of film thicknesses L_z that can reasonably be treated within the GDM, i.e. L_z should be larger than a few times the radius of gyration.

To further quantify the order in the film and its evolution following a quench from a random initial state, we introduce the time-dependent lateral structure factor

$$S(\vec{k}_{\parallel}, z, t) = \frac{L_z}{MN_A} \langle |\rho_A(\vec{k}_{\parallel}, z, t)|^2 \rangle \quad (17)$$

defined in terms of lateral density fluctuations

$$\rho_A(\vec{k}_{\parallel}, z, t) = \int d^2x_{\parallel} \rho_A(\vec{x}, t) e^{i\vec{k}_{\parallel} \cdot \vec{x}_{\parallel}} \quad (18)$$

with $\vec{x}_{\parallel} = (x, y)$. The prefactor L_z in (17) is introduced in order to achieve L_z -independence of (17) in the bulk limit $L_z \rightarrow \infty$ for given total monomer concentration. Averaging (17) over \vec{k}_{\parallel} with $k_{\parallel} = (k_x^2 + k_y^2)^{1/2}$ fixed and subsequent averaging over z yields the quantity

$S(k_{\parallel}, t)$ which is plotted in Fig. 9b. It clearly reflects lateral ordering induced by the alignment effect described above, with some initial coarsening. During the coarsening the position of the maximum $k_{\parallel}^*(t)$ approaches a non-zero value, corresponding to the lamellar distance in the equilibrium state. The structure is in fact close to the structure found in the bulk in Fig. 5b. In particular, a 3rd-order peak appears, reflecting a well ordered lamellar structure perpendicular to the walls.

The situation changes when considering an A-attractive wall, caused by a stronger repulsion for B than for A monomers,

$$\epsilon_X^{(1)} = \epsilon_X^{(2)} = \epsilon_w(1 + \delta_w^X) \quad (19)$$

where $\epsilon_w = 1$ as before and $\delta_w^B = -\delta_w^A = \delta_w > 0$. Choosing $\delta_w = 0.5$, the energetic preference of A-monomers is strong enough to overcome the essentially entropic alignment effect discussed before that molecules near the wall have reduced orientational degrees of freedom. In Fig. 10a the corresponding A-monomer density $\rho_A(z)$ is plotted across a film of thickness $L_z = \lambda$ (with λ from the corresponding bulk simulations). Layers of A-monomers adjacent to the walls rapidly form and get separated by a B-rich domain. When the wall at $z = L_z$ is replaced by a neutral one ($\epsilon_A^{(2)} = \epsilon_B^{(2)} = 1$), the equilibrium density profile essentially remains symmetric, see Fig. 10b. Thus the A-attractive wall induces layering almost as in Fig. 10a. Development of the A-rich layer near the neutral wall, however, takes much longer time than in Fig. 10a. The whole situation is reminiscent of wall-induced spinodal decomposition in films of binary polymer blends, at least in its early stages.^{33,43,44}

4.2 Periodically patterned walls

In this section we study the kinetics of pattern transfer into the film. The wall near $z = L_z$ is assumed to be neutral ($\epsilon_A^{(2)} = \epsilon_B^{(2)} = 1$), while the wall near $z = 0$ has a modulation along the y -axis with period L_p ,

$$\epsilon_X^{(1)}(y) = \epsilon_w[1 + \delta_w^X \cos(k_p y)]. \quad (20)$$

Here $\epsilon_w = 2$, $\delta_w^B = -\delta_w^A = \delta_w = 0.5$, and $k_p = 2\pi/L_p$.

As long as $\chi < \chi_c$ the equilibrium state displays a periodic segregation of monomers in the y -direction confined near $z = 0$. The decay of the segregation amplitude along the z -axis reflects the correlation length of the disordered phase. On the other hand, for $\chi > \chi_c$ various scenarios of pattern-induced microphase separation emerge, depending on film thickness and on the commensurability between the two length scales L_p and λ .

Let us begin with the commensurate case $L_p/\lambda = 1$ and a thickness $L_z = \lambda$. Figure 11 shows, for $\chi = 0.45$, the time evolution of the integrated structure factor $S(k_y, z, t) = \int dk_x S(\vec{k}_{\parallel}, z, t)$. After a rapid initial growth of a peak with $k_y \simeq k_p$ near the patterned substrate,

the associated periodic structure propagates along the z -direction. Simultaneously, a broader structure develops across the slab and indicates spontaneous microphase ordering similar to bulk behavior.⁴⁵ At $t = 2 \times 10^4$ MCS, the wall-induced sharp structure dominates everywhere and has penetrated the slab nearly uniformly. A weak 3rd-order peak is clearly seen at $k_y \simeq 3k_p$. The result is an equilibrium state with nearly perfect perpendicular lamellar ordering. No changes are observed any more when going to larger times.

For a thicker film with $L_z = 1.8\lambda$, see Fig. 12, “bulk-like” ordering processes throughout the slab evolve further and more strongly interfere with the ordering wave propagating from the patterned wall. For long times the ordering wave finally succeeds to overcome the bulk-like domain structures. Equilibrium is nearly but not fully reached at $t = 4 \times 10^4$ MCS.

Now we turn to incommensurate situations. The case $L_p/\lambda = 1.1$ and $L_z = \lambda$ will be described without showing explicit results because of its similarity at long times to the commensurate case $L_p/\lambda = 1.0$ shown in Fig. 11. The main difference at shorter times is most directly observed from the structure factor $S(k_{\parallel}, t)$ defined as in Fig. 9b. In the commensurate case bulk ordering initially leads to a shoulder in $S(k_{\parallel}, t)$ next to the primary peak at k_p , which merges with it as time proceeds. On the other hand, for $L_p/\lambda = 1.1$ and $t = 200$ MCS one can identify a separate “bulk” peak. It also merges with the peak at k_p for longer times $t > 2 \times 10^4$ MCS so that the final structure corresponds to complete penetration of the wall pattern, as in the commensurate case. It is interesting to note that transient coexistence of two peaks and final dominance of the peak at k_p have been observed recently in two-dimensional Fourier transforms of real space images of diblock copolymer thin films on chemically nanopatterned substrates.⁴⁶

By contrast, for the larger ratio $L_p/\lambda = 1.2$ with $L_z = \lambda$ the two main features in Figs. 13a - c prevailing near the patterned wall and deeper in the film, respectively, remain separated with respect to k_y as time proceeds. Up to $t = 2 \times 10^3$ MCS the peak at k_p dominates, which is evident from the averaged structure factor $S(k_{\parallel}, t)$ plotted in Fig. 14, whereas for $t > 2 \times 10^4$ MCS the quantity $S(k_{\parallel}, t)$ takes its maximum at the bulk value $k_0 = 2\pi/\lambda$. No further change of this pattern is observed in our longest runs up to $t = 6 \times 10^4$ MCS, nor does it change when we increase the strength in the modulation of the wall potential to $\delta_w = 0.75$. Hence it appears that no well-ordered structure develops in this case, showing that transfer of the wall pattern to the film sensitively depends on the commensurability of the two length scales L_p and λ .

5 Summary and Outlook

The Gaussian disphere model (GDM) provides a highly coarse grained description of diblock copolymer melts at

the molecular level which still captures the essential features of self-organized structure formation. The essence of the model is to parameterize the internal molecular degrees of freedom by a few stochastic variables, the radii of gyration R_A and R_B of each block and the distance vector \vec{r} . Molecular positions together with these internal variables move according to a kinetic MC algorithm. The algorithm is driven by a free energy $F(\{\vec{r}_i\}, \{R_i^A\}, \{R_i^B\})$ derived from Gaussian chains, in analogy to the Gaussian ellipsoid model for polymer melts proposed earlier.^{6,7}

Regarding bulk ordering and diffusion, several features known from less coarse grained models were reproduced to a good approximation. This prompted us to study microphase ordering in thin films, especially the kinetics of pattern transfer from a stripe-patterned substrate into the film. Detailed results for the time-dependent structure factor $S(k_y, z, t)$ were presented, including some discussion of commensurability effects and pattern penetration into films of varying thickness.

The GDM is expected to lose reliability, when the

film thickness becomes less than a few times the radius of gyration. Then the assumed sphericity of individual blocks is no longer compatible with the molecules' distortion under confinement. Improvement on that issue could be achieved in the spirit of Ref.⁷ by allowing ellipsoidal block shapes or by representing each block as a string of soft spheres.

On the other hand, the GDM may turn out advantageous in a semi-quantitative description of more complex molecules, including chain-like segmented or branched copolymers, or copolymers carrying reactive groups.⁴⁷

Acknowledgement

Financial support by the Deutsche Forschungsgemeinschaft (International Research Training Group "Soft condensed matter") and the UFA (Université Franco Allemande) is gratefully acknowledged.

-
- ¹ K. Binder, Adv. Pol. Science **112**, 181 (1994).
² M. Böltau, S. Walheim, J. Mlynek, G. Krausch and U. Steiner, Nature **391**, 877 (1998).
³ J. Baschnagel and K. Binder, Macromolecules **28**, 6808 (1995).
⁴ C. N. Likos, Physics Reports **348**, 267 (2001).
⁵ M. Murat and K. Kremer, J. Chem. Phys. **108**, 4340 (1998).
⁶ F. Eurich and P. Maass, J. Chem. Phys. **114**, 7655 (2001).
⁷ F. Eurich, P. Maass and J. Baschnagel, J. Chem. Phys. **117**, 4564 (2002).
⁸ G. Yabenko, E. I. Sambriski, M. A. Nemirovskaya, and M. Guenza, Phys. Rev. Lett. **93**, 257803 (2004).
⁹ G. Yabenko, E. I. Sambriski, and M. Guenza, J. Chem. Phys. **122**, 054907 (2005).
¹⁰ F. S. Bates and G. H. Fredrickson, Phys. Today **52**, 32 (1999).
¹¹ M. W. Matsen, J. Phys.: Condens. Matter **14**, R21 (2002).
¹² G. Srinivas, D. E. Discher, and M. L. Klein, Nature Mater. **3**, 638 (2005).
¹³ D. Zschech, D. H. Kim, A. P. Milenin, S. Hopfe, R. Scholz, P. Göring, R. Hillebrand, S. Senz, C. J. Hawker, T. P. Russel, M. Steinhart, and U. Gösele, Nanotechnology **17**, 2122 (2006).
¹⁴ L. Leibler, Macromolecules **13**, 1602 (1980).
¹⁵ T. Ohta and K. Kawasaki, Macromolecules **19**, 2621 (1986).
¹⁶ G. H. Fredrickson and E. Helfand, J. Chem. Phys. **87**, 697 (1987).
¹⁷ H. Fried and K. Binder, J. Chem. Phys. **94**, 8349 (1991).
¹⁸ A. Hoffmann, J.-U. Sommer, and A. Blumen, J. Chem. Phys. **106**, 6709 (1997).
¹⁹ A. Hoffmann, J.-U. Sommer, and A. Blumen, J. Chem. Phys. **107**, 7559 (1997).
²⁰ G.S. Grest, M.-D. Lacasse, K. Kremer, and A. M. Gupta, J. Chem. Phys. **105**, 10583 (1996).
²¹ M. Murat, G. S. Grest, and K. Kremer, Europhys. Lett. **42**, 401 (1998).
²² M. Murat, G. S. Grest, and K. Kremer, Macromolecules **32**, 595 (1999).
²³ A. J. Schultz, C. K. Hall and J. Genzer, J. Chem. Phys. **117**, 10329 (2002).
²⁴ R. D. Groot and T. J. Madden, J. Chem. Phys. **108**, 8713 (1998).
²⁵ R. D. Groot, T. J. Madden, and D. J. Tildesley, J. Chem. Phys. **110**, 9739 (1999).
²⁶ Y. Masubuchi, G. Ianniruberto, F. Greco, and G. Marrucci, J. Non-Cryst. Solids **352**, 5001 (2006).
²⁷ N. M. Maurits and J. G. E. M. Fraije, J. Chem. Phys. **107**, 5879 (1997).
²⁸ M. Nonomura, K. Yamada and T. Ohta, J. Phys: Condens. Matter **15**, L423 (2003).
²⁹ A. Chakrabarty, R. Toral, and J. D. Gunton, Phys. Rev. A **44**, 6503 (1991).
³⁰ J. G. E. M. Fraije, B. A. C. van Vlimmeren, N. M. Maurits, M. Postma, O. A. Evers, C. Hoffmann, P. Altevogt, and G. Goldbeck-Wood, J. Chem. Phys. **106**, 4260 (1997).
³¹ M. W. Matsen, Phys. Rev. Lett. **74**, 4225 (1995).
³² S. Ludwigs, G. Krausch, R. Magerle, A. V. Zvelindovsky and G. Sevink, Macromolecules **38**, 1859 (2005).
³³ F. Eurich, "Coarse-grained models for the kinetics of polymeric systems", thesis, Universität Konstanz (Verlag im Internet GmbH, Berlin, 2002).
³⁴ W. Dieterich, I. Peschel, and W. Schneider, Z. Physik **B27**, 177 (1977).
³⁵ U. Thomas and W. Dieterich, Z. Physik B-Condensed Matter **62**, 287 (1986).
³⁶ J.-L. Barrat and G. H. Fredrickson, Macromolecules **24**, 6378 (1991).
³⁷ K. Binder, Adv. Pol. Science **138**, 1 (1999).
³⁸ J.-U. Sommer, A. Hoffmann and A. Blumen, J. Chem. Phys. **111**, 3728 (1999).
³⁹ M. Kikuchi and K. Binder, J. Chem. Phys. **101**, 3367 (1994).
⁴⁰ L. Rockford, Y. Liu, P. Mansky, T. P. Russell, M. Yoon and S. G. J. Mochrie, Phys. Rev. Lett. **82**, 2602 (1999).

- ⁴¹ Q. Wang, Qiliang Yan, P. F. Nealey and J. J. de Pablo, *Macromolecules* **33**, 4512 (2000).
- ⁴² H. Chen and A. Chakrabarty, *J. Chem. Phys.* **108**, 6897 (1998).
- ⁴³ S. Puri and H.L. Frisch, *J. Phys.: Condens. Matter* **9**, 2109 (1997).
- ⁴⁴ H. P. Fischer, P. Maass and W. Dieterich, *Europhys. Lett.* **42**, 49 (1998); H. P. Fischer, P. Maass and W. Dieterich, *Phys. Rev. Lett.* **79**, 893 (1997).
- ⁴⁵ At early times a smaller peak in $S(k_p, z, t)$ and a well defined minimum near $z \approx 2\langle(R^A)^2\rangle^{1/2} \approx 7.2$ can be observed in between these two main features. This secondary peak results from AABB block sequences (at fixed z) due to molecules in the second layer from the wall, with preferential perpendicular orientation. This is inferred from the z -dependence of $\langle|\cos \Theta(z)|\rangle$.
- ⁴⁶ E. W. Edwards, M. P. Stoykovich, M. Müller, H. H. Solak, J. J. De Pablo and P. F. Nealey, *J. Polymer Science B* **43**, 3444 (2005).
- ⁴⁷ I. Krakovsky, J. Plestil, J. Baldrian, and M. Wübbenhorst, *Polymer* **43**, 4989 (2002).

TABLE I: Parameters for fitting the generalized Leibler function (13) to structure factor data in Fig. 3.

χN	0.0	2.5	5.0	10.0	12.5	15.0
α	1.9	1.8	1.9	1.6	1.4	1.5
δ	2.1	6.4	8.9	15.5	17.9	19.2
\tilde{R}_G	6.1	6.1	6.3	6.3	6.4	6.5

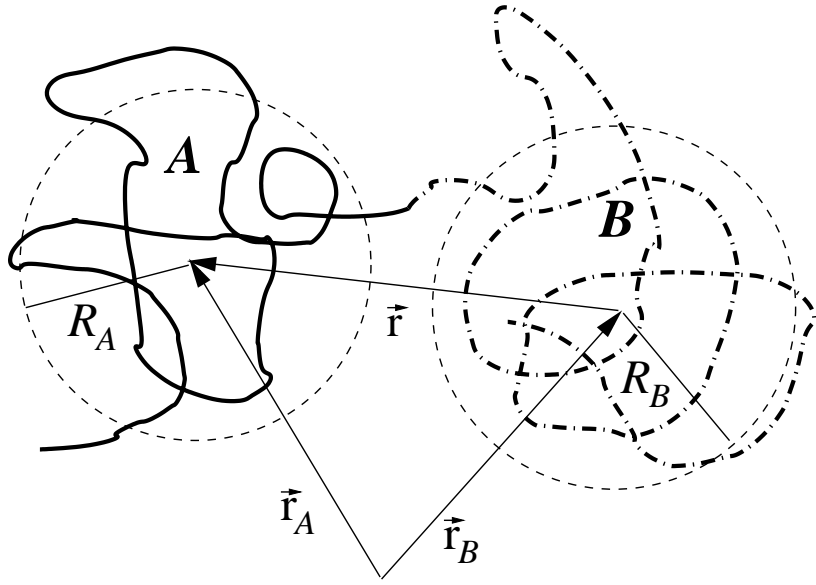


FIG. 1: Schematic illustration of the Gaussian disphere model.

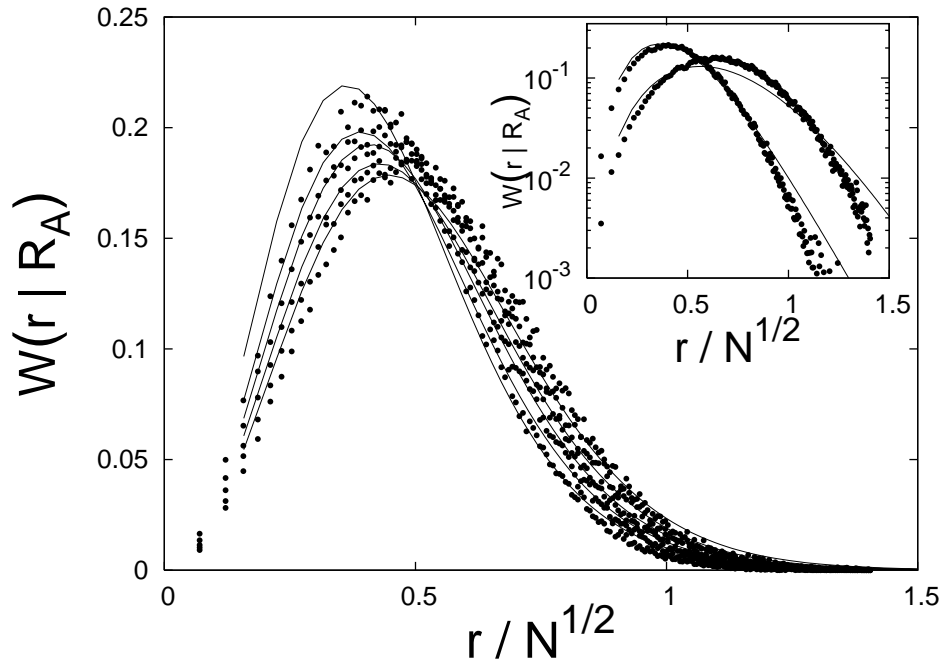


FIG. 2: Comparison between the conditional probability $W(r|R^A)$ based on the Gaussian approximation (9) (continuous curves) with Monte Carlo data for symmetric chains with $N = 100$. To display the dependence on R_A , averages have been taken over eight successive (R^A) -intervals, see text. Different curves refer to the first five of these intervals. With increasing R^A -values, distributions $W(r|R^A)$ shift towards larger r -values. The inset shows, in a semi-logarithmic representation, the results for the smallest and largest of these eight (R^A) -intervals, confirming that the Gaussian approximation is satisfactory as long as $r \lesssim N^{1/2}$.

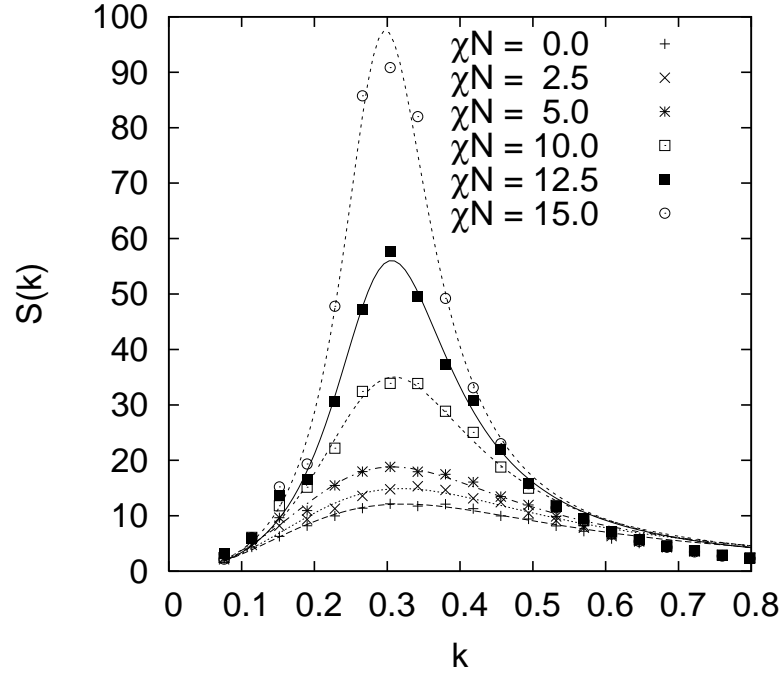


FIG. 3: Simulated structure factor $S(k)$ in the disordered phase for different χN . Continuous curves are fits to Eq. (13).

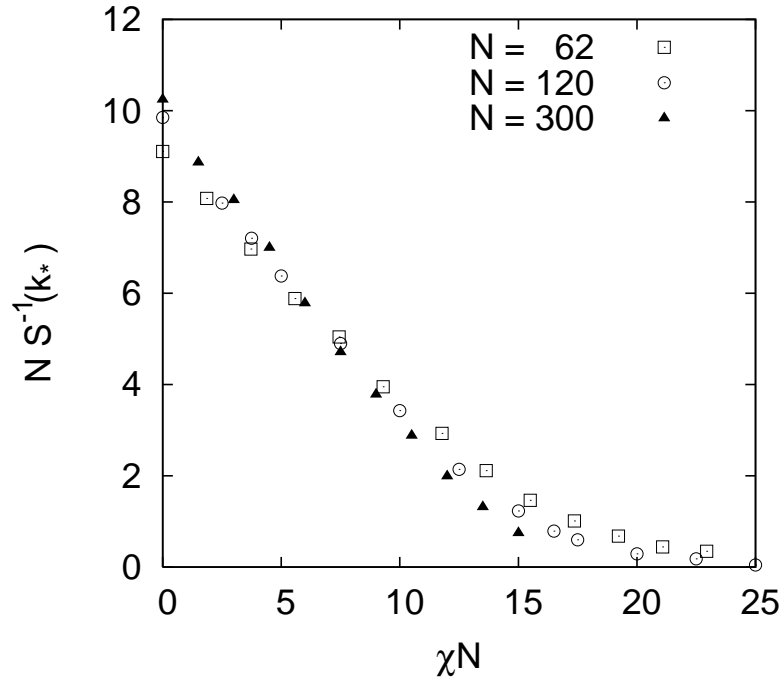


FIG. 4: Normalized inverse maximum of the structure factor versus χN for three different chain lengths.

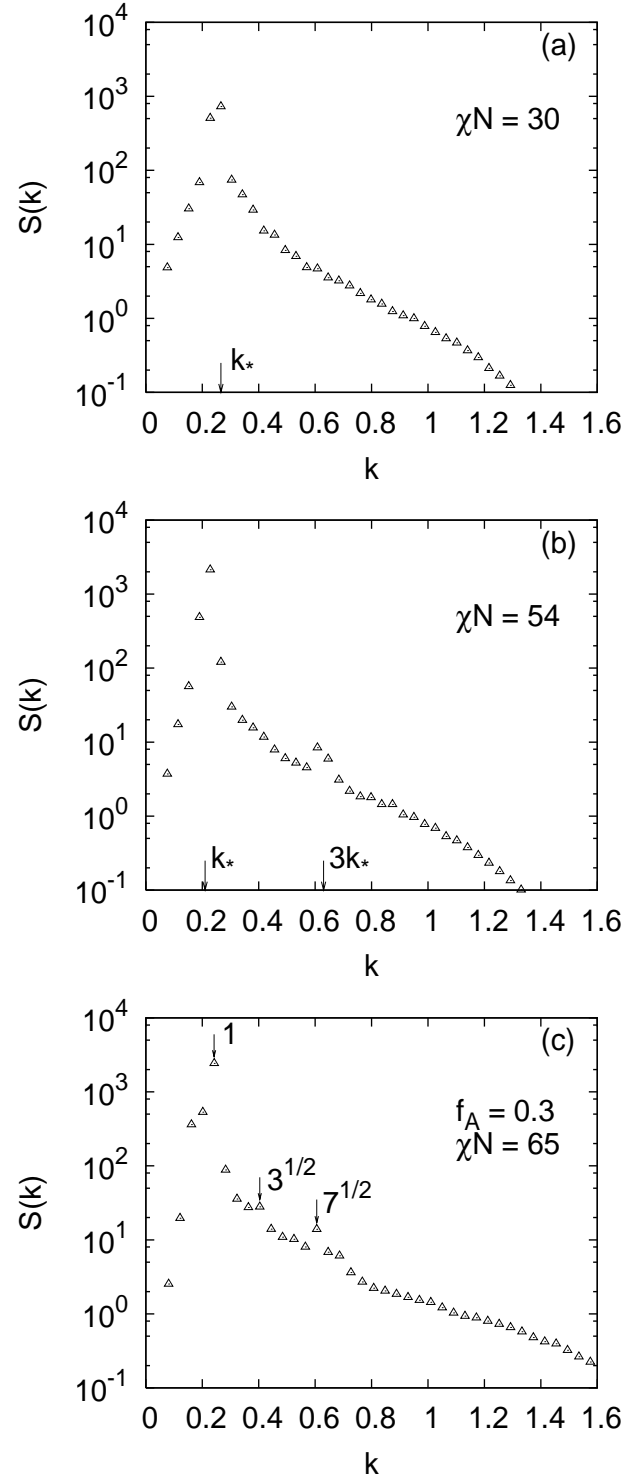


FIG. 5: Spherically averaged structure factor in ordered phases. Lamellar phase with (a) $\chi N = 30$ (weak segregation) and (b) $\chi N = 54$ (strong segregation), displaying the third order peak. (c) Cylindrical phase with $f_A = 0.3$, $\chi N = 65$ ($N = 100$), with marked higher order peaks.

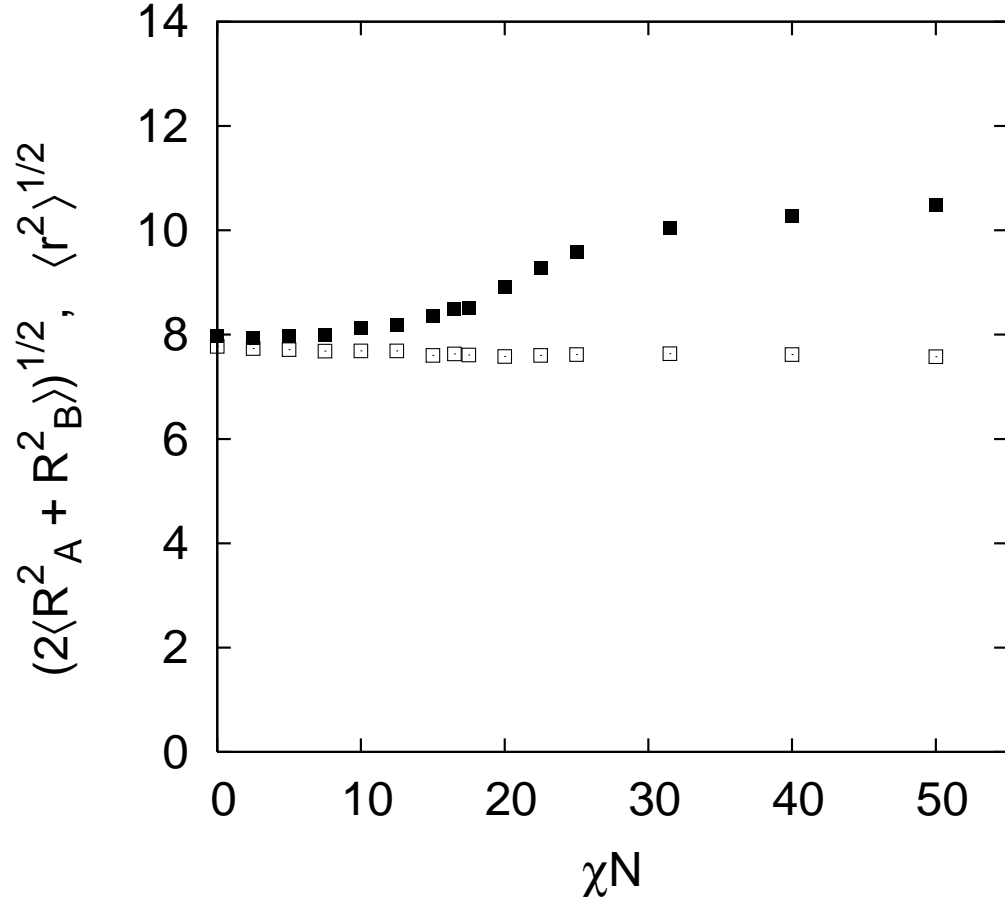


FIG. 6: Averaged stretching parameter r (full symbols) compared to averaged radii of gyration $\langle (R^A)^2 \rangle^{1/2} = \langle (R^B)^2 \rangle^{1/2}$ (light symbols), cf. Eq. (9), versus χN .

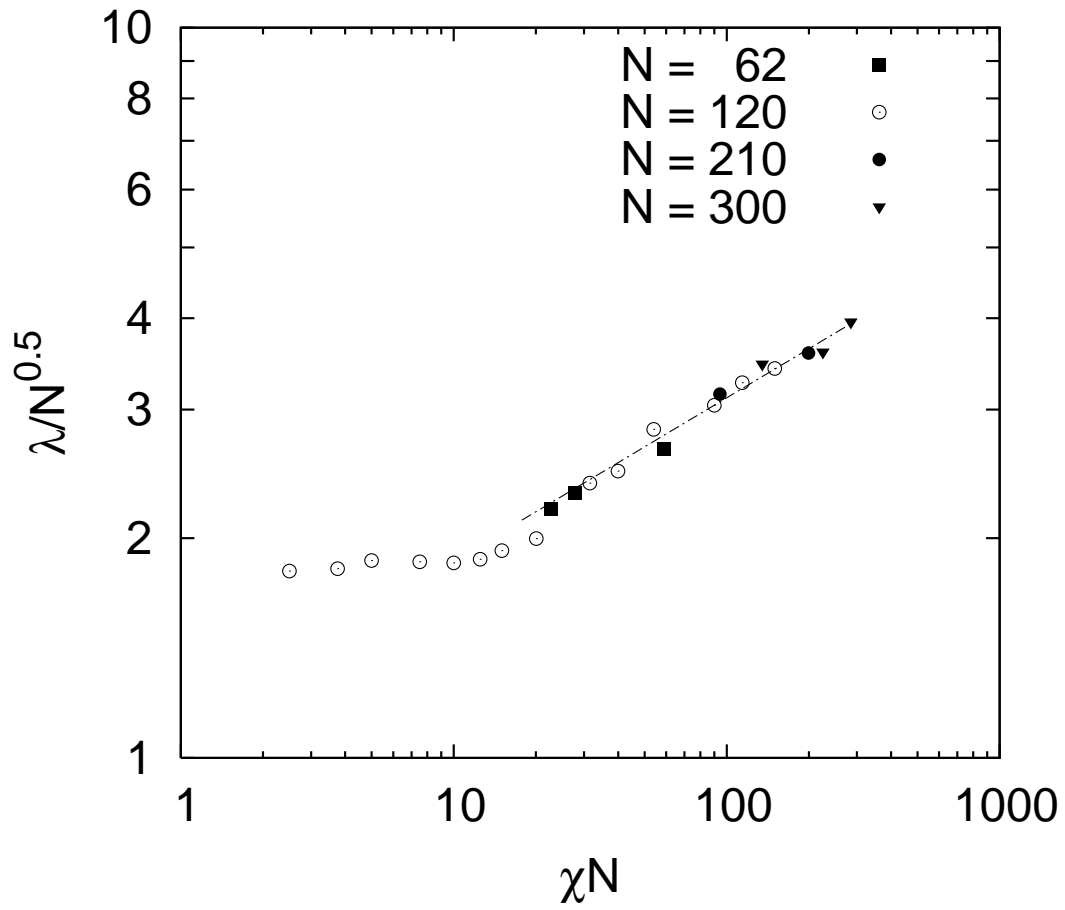


FIG. 7: Scaling plot of lamellar distance λ depending on χ and N extending to the strong segregation-regime. The dashed straight line has a slope $n \simeq 0.22$. Data points for $N = 120$ are continued to the disordered phase. In these simulations, averages were taken over three independent runs.

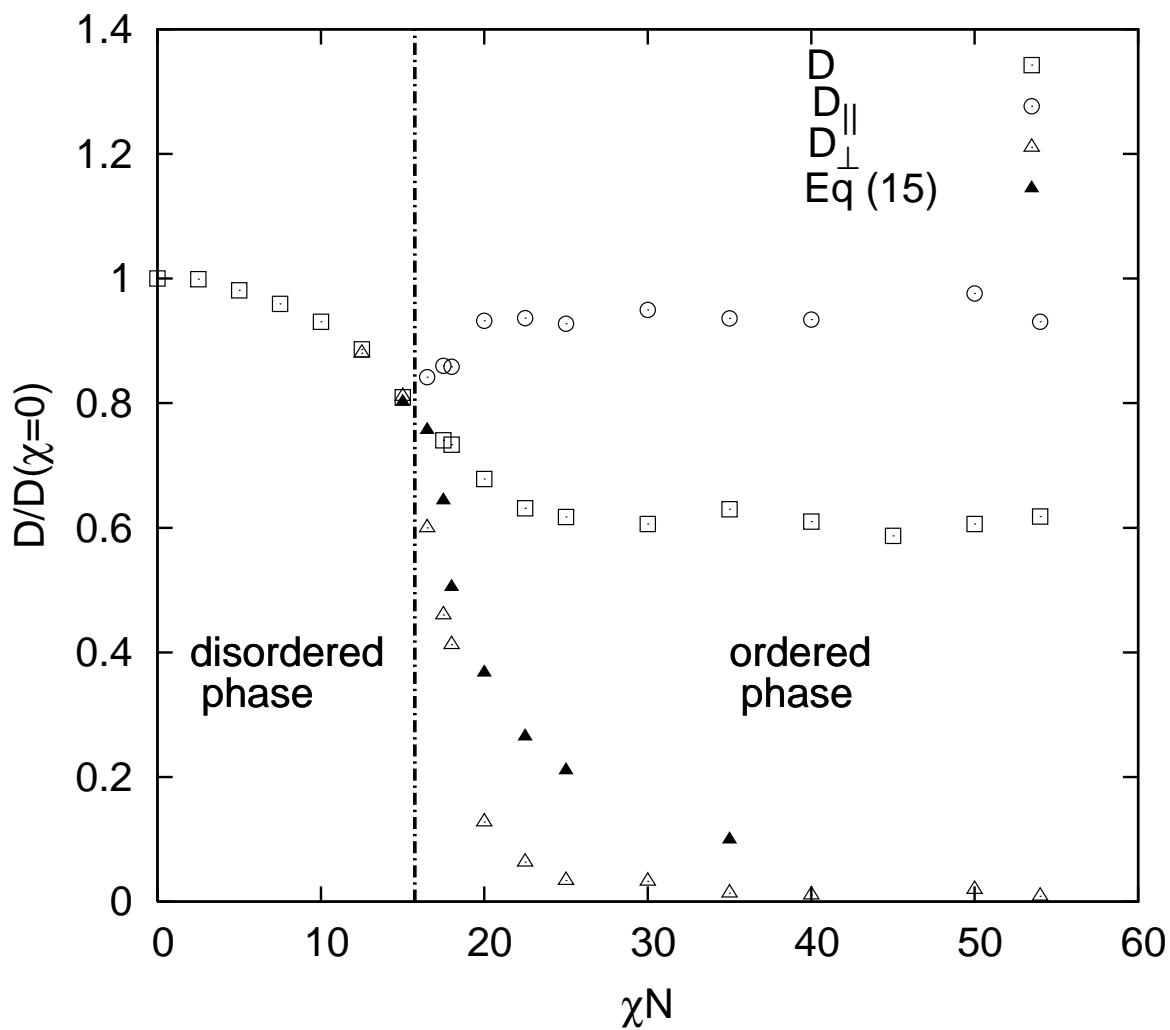


FIG. 8: Normalized diffusion coefficient D as well as anisotropic diffusion coefficients D_{\parallel}, D_{\perp} in the lamellar phase, versus χN . The vertical dashed dotted line separates isotropic from anisotropic diffusion. Its position agrees with estimates for the ordering transition based on equilibrium simulations (section 3.1).

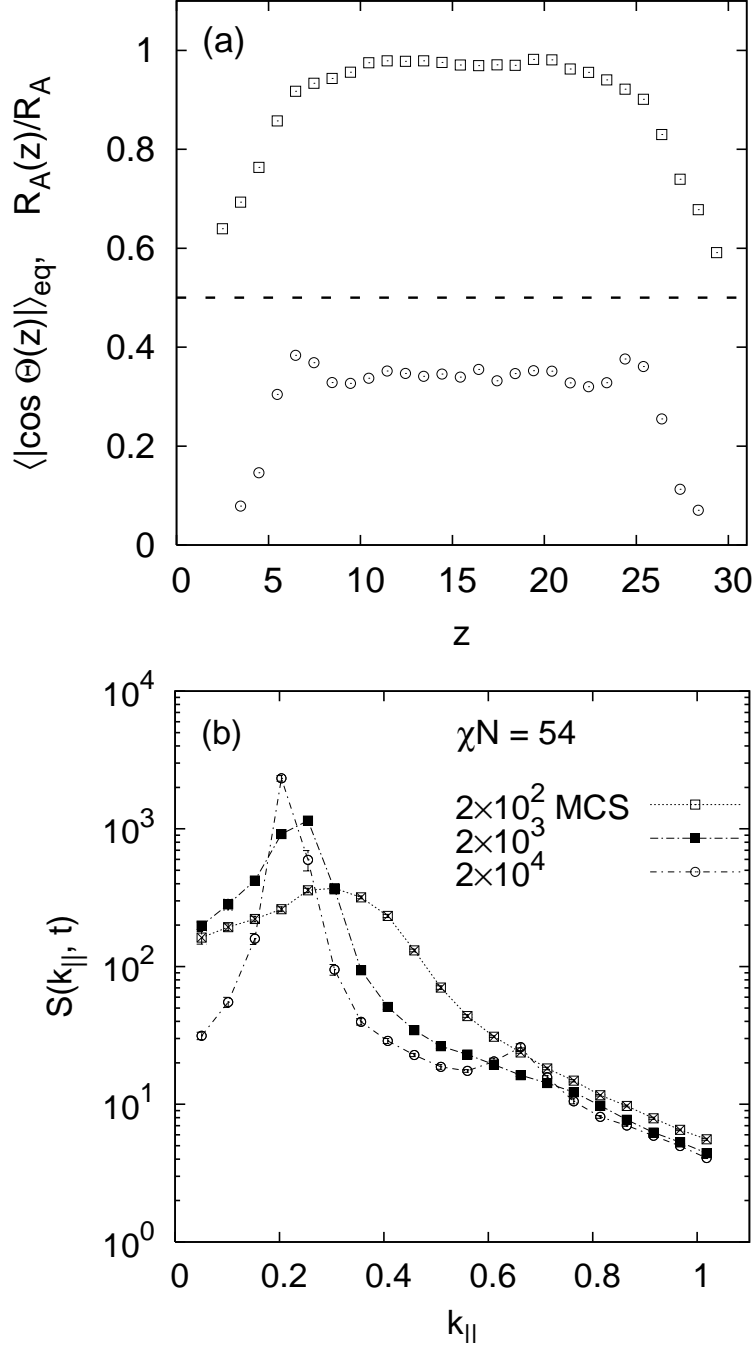


FIG. 9: (a) Wall-induced molecular orientation (circles) and normalized radius of gyration $R_A(z) = \langle R_A^2(z) \rangle^{1/2}$ (squares) of blocks across the slab for $\chi = 0.45$. The horizontal dotted line corresponds to random orientation, $\langle |\cos \Theta(z)| \rangle = 1/2$. The grid size along the z -axis is $\Delta z = 1$. Chosen parameters are $f_A = 0.5$, $\chi = 0.45$ and $N = 120$. (b) Time evolution of circularly averaged structure factor after averaging over z . Note the appearance of the 3rd-order peak in the final equilibrated state.

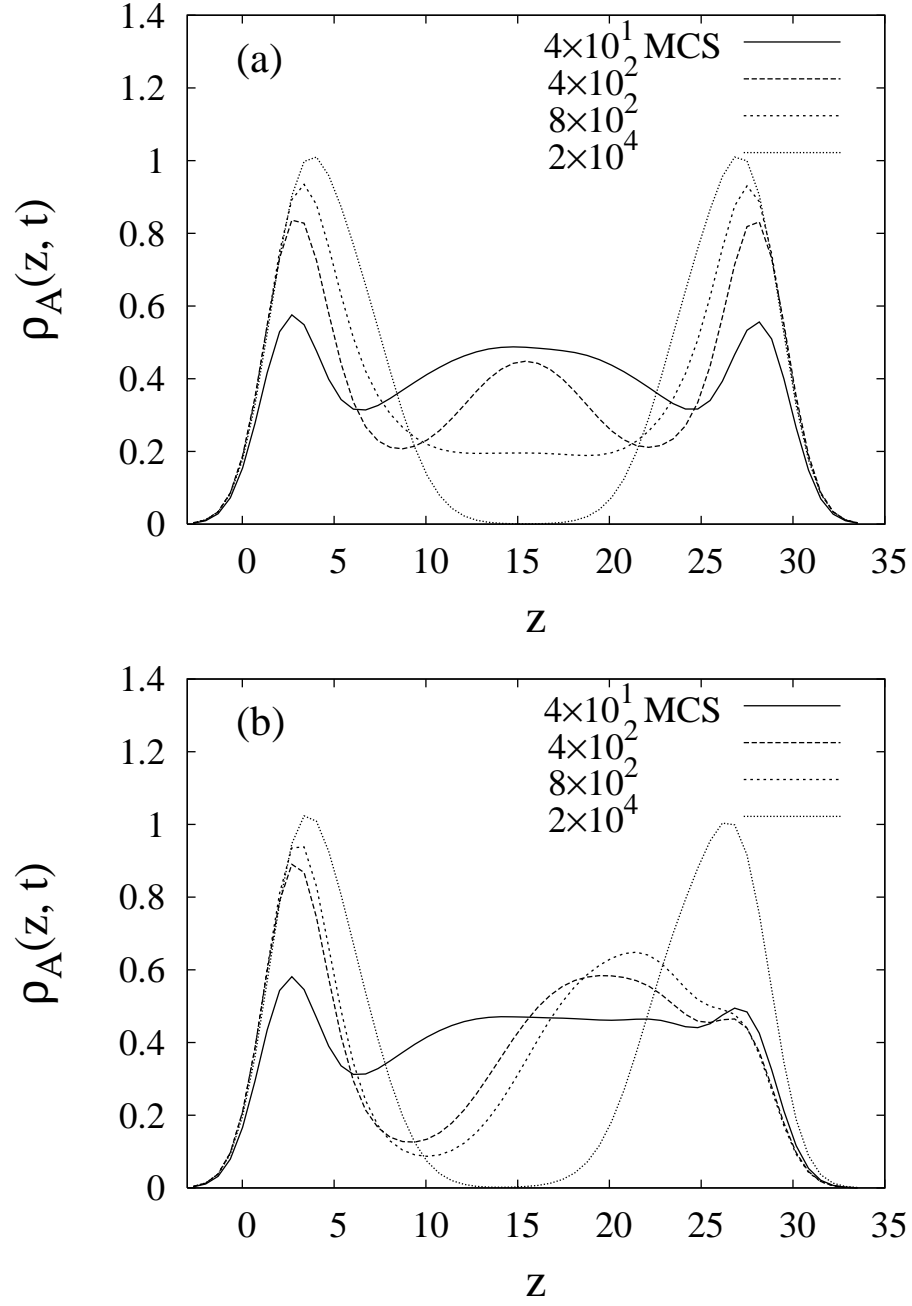


FIG. 10: (a) Time evolution of the A-monomer density in a film of thickness $L_z = \lambda$ with A-attractive walls, for $\chi = 0.45$ (b) Same, but with A-attractive left and neutral right wall.

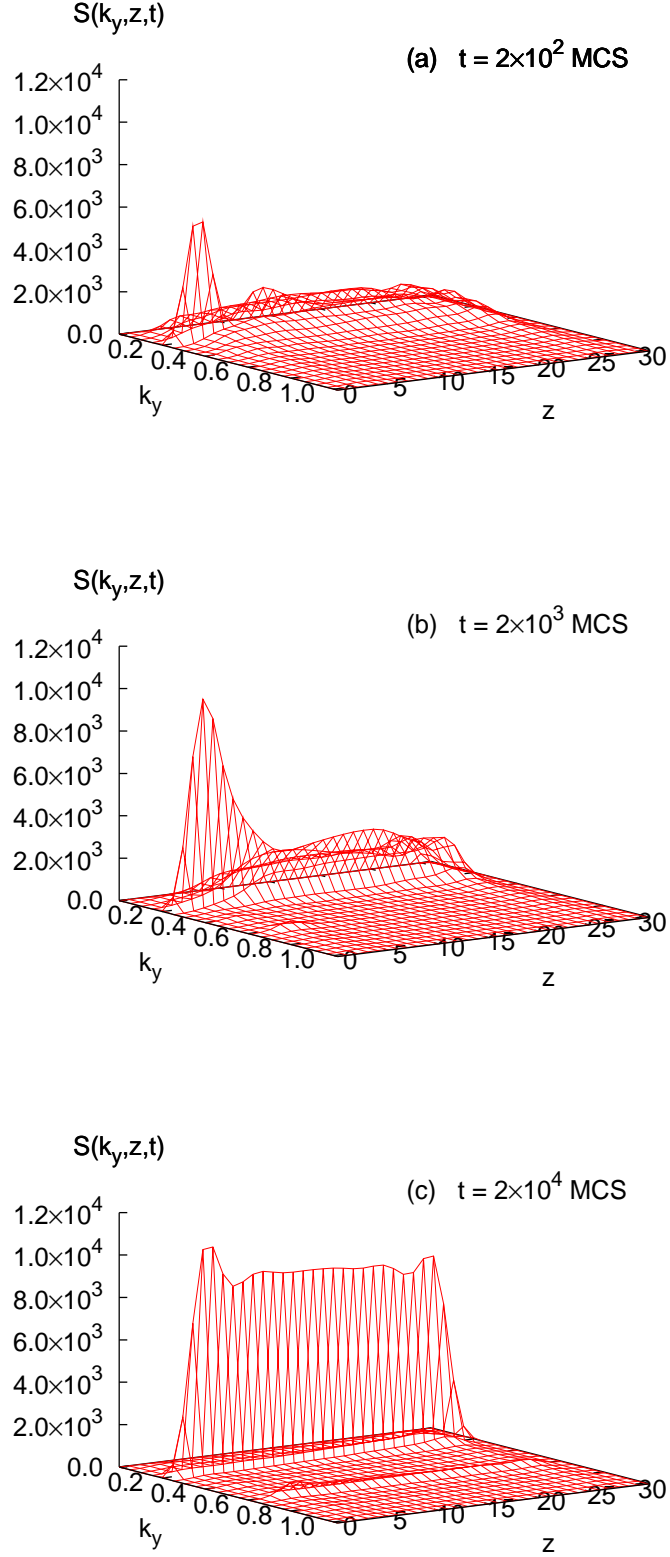


FIG. 11: Time evolution of the structure factor $S(k_y, z, t)$ in the presence of a stripe-patterned wall near $z = 0$, for $\chi = 0.45$. The pattern periodicity is $L_p = 2\pi/k_p = \lambda$ and the film thickness $L_z = \lambda$. The lateral system size is $L_x = L_y = 4L_p$. (a) $t = 200$ MCS, (b) $t = 2 \times 10^3$ MCS, (c) $t = 2 \times 10^4$ MCS.

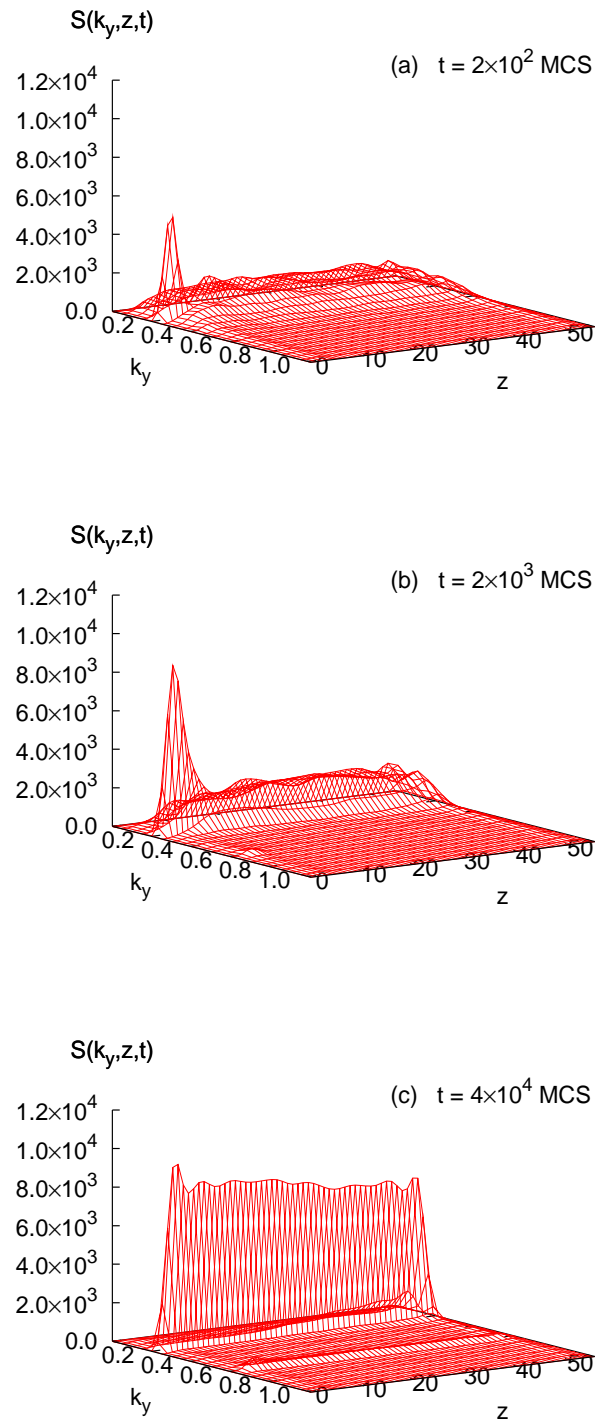


FIG. 12: Same as Fig. 11, but $L_z = 1.8\lambda$, and $t = 4 \times 10^4$ MCS in (c).

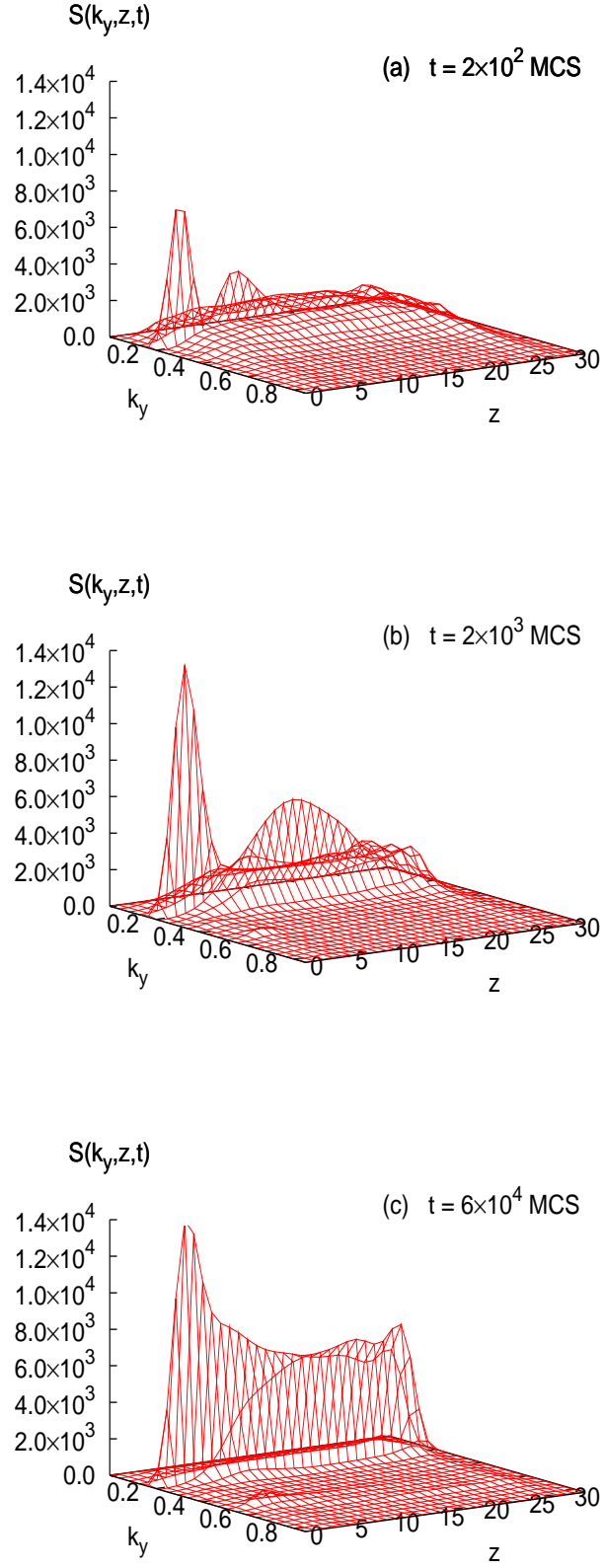


FIG. 13: Same as Fig. 11, but $L_p = 1.2\lambda$, and $t = 6 \times 10^4$ MCS in (c).

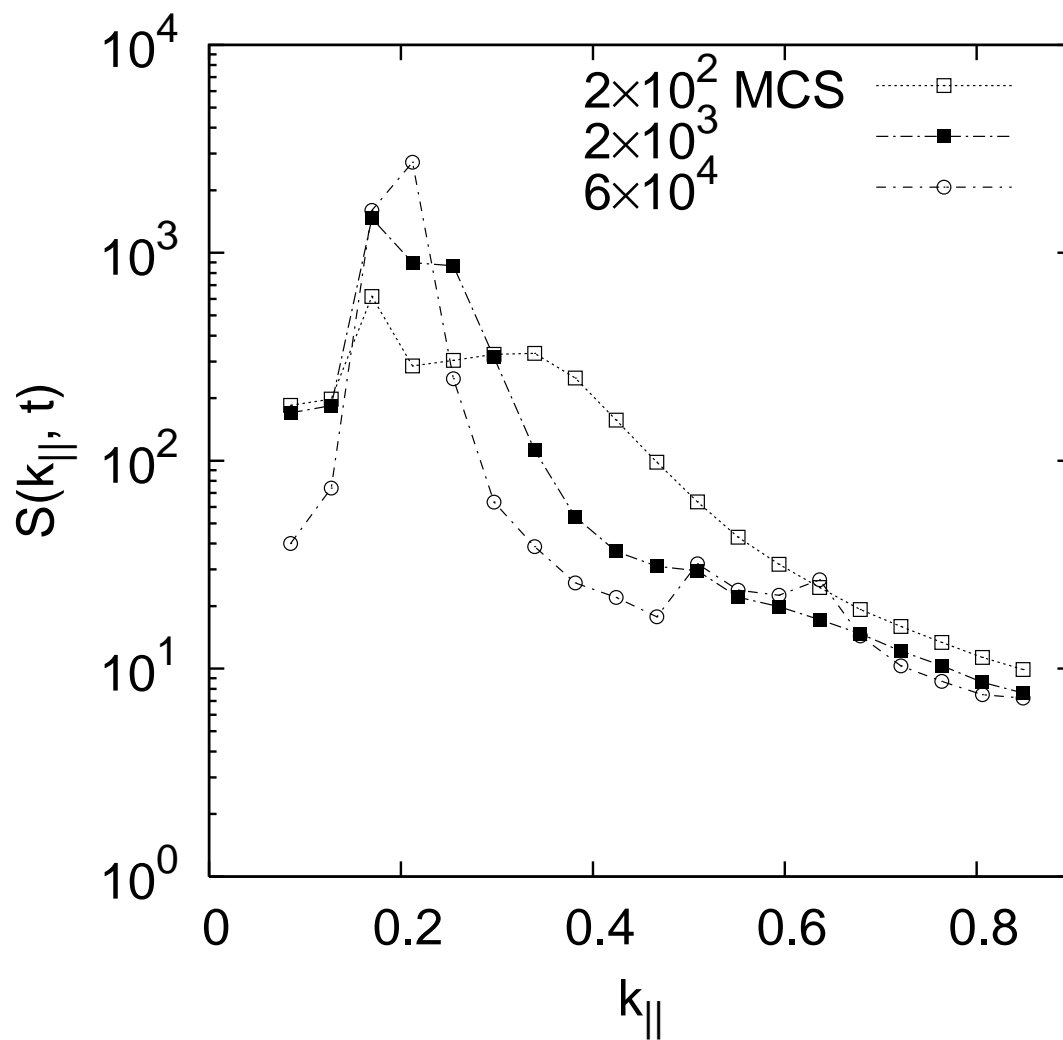


FIG. 14: Circularly and z -averaged structure factor from the same simulation data as in Fig. 13.